ACS APPLIED MATERIALS & INTERFACES

RESEARCH ARTICLE

www.acsami.org

Interfacial Reactivity of Au, Pd, and Pt on BiI_3 (001): Implications for Electrode Selection

Wei Qiu,* Gregory J. Dudder, Xueying Zhao, Scott S. Perry, and Juan C. Nino

Department of Materials Science and Engineering, University of Florida, Gainesville, Florida 32611, United States

ABSTRACT: Understanding the contact-semiconductor interface is important in determining the performance of a semiconductor device. This study investigated the contact chemistry of BiI_3 single crystal with Au, Pd, and Pt electrodes using X-ray photoelectron spectroscopy (XPS), a technique widely used to probe the interfacial chemistry of many materials. Chemical reactions were identified on the BiI_3 surface for the case of Pd and Pt contacts, while Au showed no reactivity with BiI_3. The difference in reactivities correlated with different surface morphologies of the contact on the BiI_3 surface, which was evidenced by atomic force microscopy (AFM) characterization. The dark resistivity of the BiI_3 crystal with above contact materials was measured by I−V characterization. The highest resistivity was obtained when Au was employed as the contact. These results suggest that Au is better than Pd and Pt as the contact material for BiI_3 single crystal.

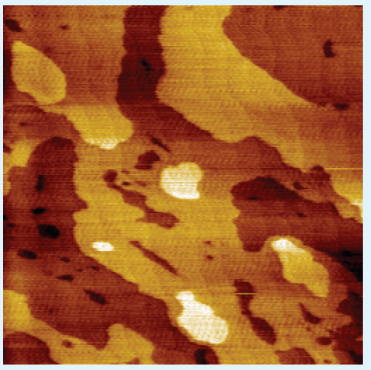

KEYWORDS: BiI_3, XPS, contact, electrode, reactivity, AFM

1. INTRODUCTION

Bismuth tri-iodide (BiI_3) is a semiconductor material that has been studied as a promising candidate for room temperature gamma-ray detection applications.[1,2] BiI_3 crystallizes in a rhombohedral structure (space group, $R\bar{3}$, No. 148) with six formula units per unit cell. The lattice parameters of BiI_3 are a = 7.519 Å and c = 20.720 Å. Each unit cell consists of three I−Bi−I layers stacked along [00l] direction. Within each layer the Bi and I form strong ionic bonds, however, only weak van der Waals forces hold the layers together. This layered structure leads to BiI_3 crystals being easily cleaved perpendicular to their [00l] directions. For detector fabrication, a conductive contact has to be applied on the surface of BiI_3. A good contact material should be nonreactive with the semiconductor and will not create additional defects at the contact-semiconductor interface.[3,4] Though Au and Pd have both been used as contacts for BiI_3 single crystals[1,2,5] and polycrystalline films,[6] the reactivity of metal contacts over BiI_3 has never been reported and the ideal contact material for the detector application has yet to be identified.

The contact-semiconductor interface plays an important role in detector applications. A chemically and mechanically stable contact is always desired for radiation detectors.[7] Chemical and strong physical interactions between the contact and the semiconductor are often found to degrade the detector performances.[7−10] For example, HgI_2 detectors employing Cu as the electrode have very poor performance and high leakage currents because of Cu diffusion in HgI_2.[8] Ag and Al have been found to be devastating to HgI_2 detectors due to severe interfacial chemical reactions.[9,10] Therefore, the investigation of contact chemistry for detectors of various compositions is critical for proper detector development.

X-ray photoelectron spectroscopy (XPS) has been widely used to probe metal-semiconductor interfaces, and has proved useful in describing the details of interfacial chemistry in these systems.[11−14] In this study, the contact chemistry of BiI_3 has been investigated with the contact materials Au, Pd, and Pt. The contact-BiI_3 interfaces have been studied by XPS and atomic force microscopy (AFM) and compared in terms of BiI_3 single crystals dark resistivity, as measured with the different contact materials.

2. EXPERIMENTAL PROCEDURES

BiI_3 single crystals were grown by a modified vertical Bridgman method. For the crystal growth, BiI_3 powder (99.999%, MV Laboratories) was vacuum sealed in a 3/4" diameter borosilicate glass ampule at a pressure of approximately 10^{-5} Torr. The ampule was placed vertically in a programmable 24 heating zone vertical furnace (EDG-13, Mellen Company). A temperature profile was pre-established in the furnace with the temperature gradient of 10 °C/cm at the solidification frontier. During crystal growth, the temperature profile was controlled to move along the vertical axis with a speed of 0.5 mm/h. This simulates the ampule movement in the conventional vertical Bridgman method. A polycrystalline ingot was obtained after the growth and single crystals were cleaved perpendicular to the [001] direction from the ingot. The crystals for XPS characterization were cut with a surface dimension of 1 by 1 cm. The (001) surface of the as grown BiI_3 single crystal was prepared by peeling off its top layer using Scotch tape, and stored in a N_2 purged drybox overnight. The cleaved surface was sputter coated with Au, Pd, or Pt metal using a Kurt J. Lesker CMS-18 multi target sputter system, resulting in a film thickness around 1 nm. The sputtering was conducted in a vacuum chamber with a pressure of 10^{-8} Torr, at a deposition speed of approximately 0.5 nm/s at room temperature. A freshly cleaved surface of a BiI_3 single crystal was used as a reference. The crystal surface exposed in air for one month was also studied to check its stability in ambient environment.

Received: January 27, 2011
Accepted: May 6, 2011
Published: May 06, 2011

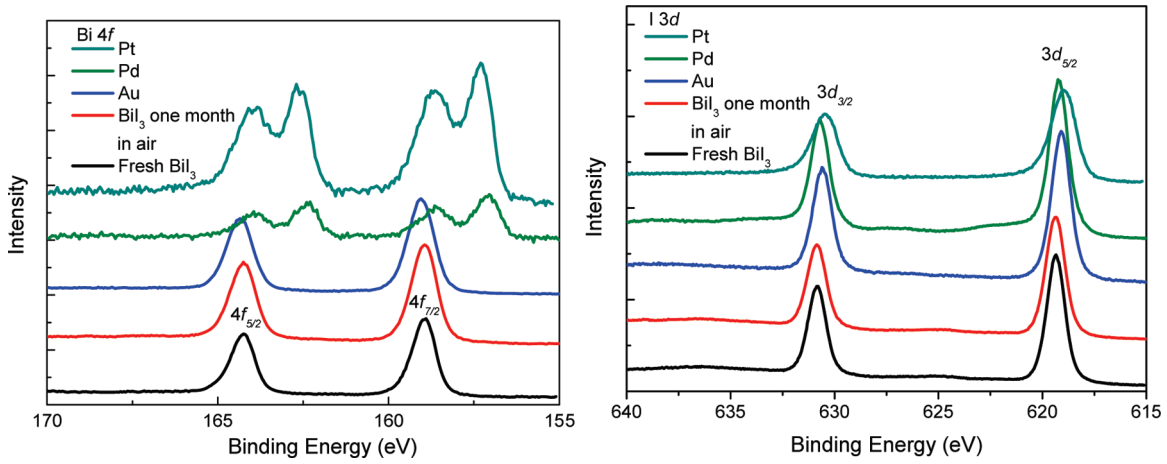

Figure 1. XPS spectra of Bi 4*f* and I 3*d* for the freshly cleaved BiI_3 (001) surface, surface exposed in air for one month, and surface with Au, Pd, and Pt electrode.

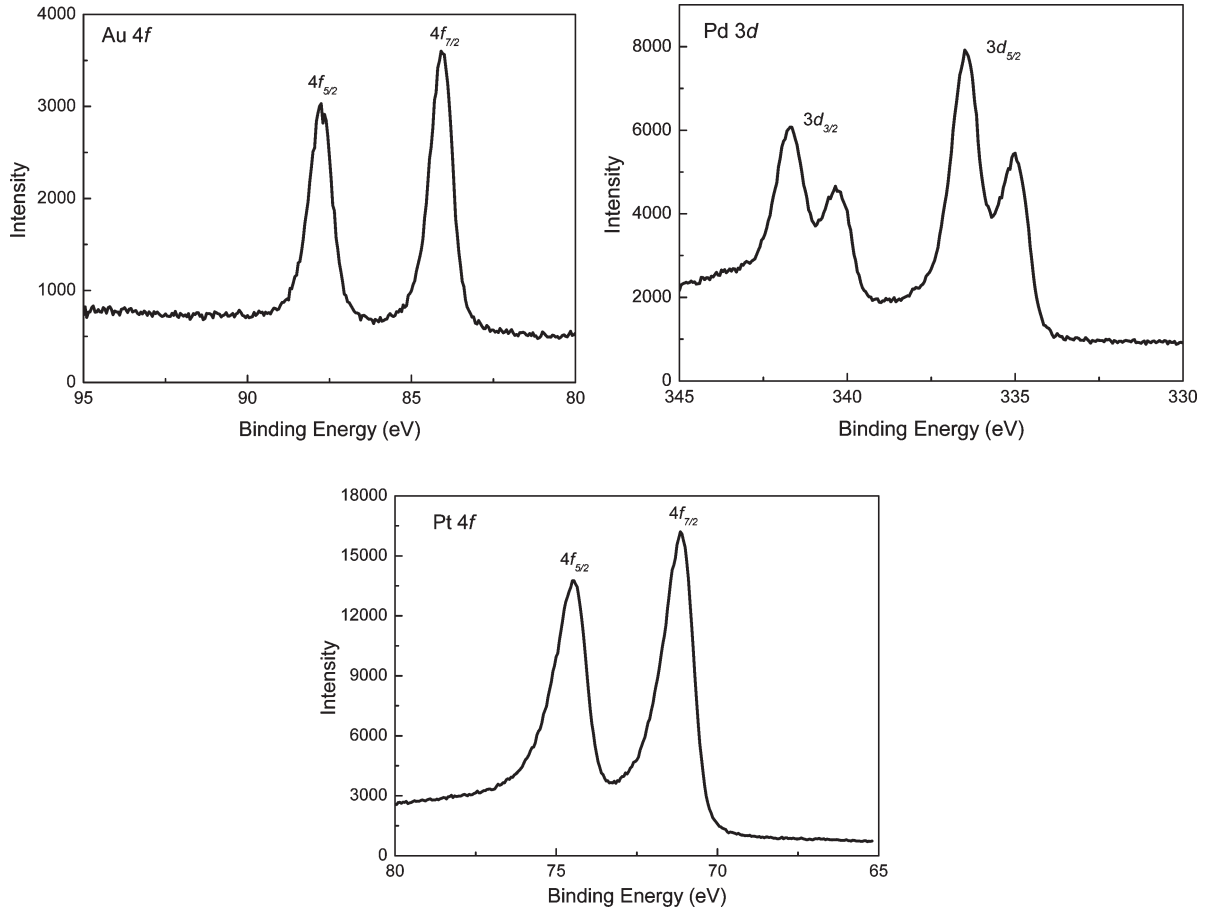

Figure 2. X-ray photoelectron spectra of Au 4*f*, Pd 3*d*, and Pt 4*f* on the surface of BiI_3 single crystals with Au, Pd, and Pt electrode.

X-ray photoelectron spectra were collected with an Omicron XPS system and an Al Kα monochromatic X-ray source (1486.7 eV). The chamber pressure was kept below 3.75×10^{-10} Torr during measurement. The instrument resolution was <0.1 eV. The instrument was calibrated using a 99.99% pure Ag sample to measure a Ag $3d_{5/2}$ peak at 368.30 eV. The spectra were recorded with a rectangular sampling area of 1.3 mm^2, a takeoff angle (the angle between the detector and the norm of the sample surface) of 55°, pass energy of 20 eV, and 0.05 eV step size for the bismuth 4*f*, iodine 3*d*, gold 4*f*, palladium 3*d*, platinum 4*f*, carbon 1*s*, and oxygen 1*s* core regions. Sensitivity factors for quantitative analysis were taken from the PHI XPS Handbook and assumed a 90 degree relationship between the incident X-rays and the electron analyzer.[15] A Shirley background subtraction method was used to eliminate the contribution of inelastic interaction intensities.[16] The 3*d* and 4*f* peak splitting was fixed to a 3:2 and 4:3 area ratio, respectively. All peaks within a core region were constrained to have the same fwhm value and

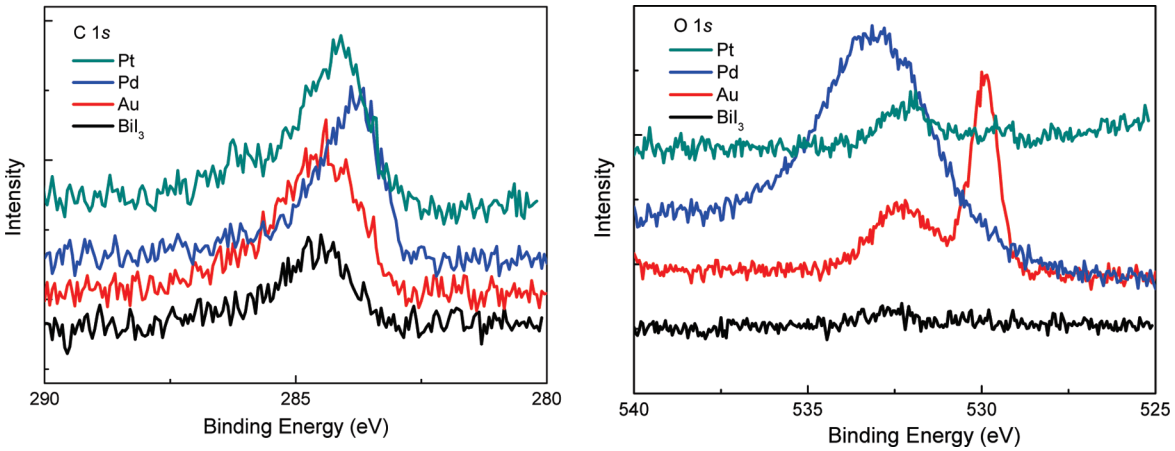

Figure 3. X-ray photoelectron spectra of C 1*s* and O 1*s* for all the samples.

were treated with a 90% Gaussian, 10% Lorentzian shape. A fitting algorithm, minimizing the squared sum of the difference between the constructed peaks and the measured spectrum, was used to finalize the overall peak fit spectrum. Fitting was considered complete when the value of the standard deviation of the residual spectral difference was less than 2.0.

To investigate the surface morphology of the metal contacts, an Asylum MFP-3D research AFM was utilized. The AFM triangular cantilever (Veeco) possessed a stated nominal tip radius of 20 nm and a normal force constant of 0.58 N/m. Constant contact mode imaging was used to acquire the topography of the samples with a 10 nN normal load set point.

The resistivity of BiI_3 single crystals with different contact electrodes was studied by I−V characterization using an Agilent 4155B semiconductor parameter analyzer. For this measurement, samples were prepared by sputtering Au, Pd, or Pt onto the freshly cleaved BiI_3 surface under the same conditions described for the XPS samples and resulted in an electrode thickness of ∼200 nm. Pt wires were attached to the electrodes using silver paste (SPI Supplies) for electrical connection.

3. RESULTS AND DISCUSSION

3.1. XPS Spectra. The XPS core level spectra of all the elements detected in survey scans of the entire energy range are shown in Figure 1−3. The observed elemental binding energies are summarized in Table 1. In the following discussion, the sample with freshly cleaved surface is referred to as the BiI_3 sample; the samples with deposited metallic contacts are named Au, Pd, and Pt sample, respectively. A cursory survey of the XPS spectra reveals that the chemical states of the crystal surface remain unchanged after exposed in air for one month. The Au sample preserves the chemical state of BiI_3, while Pd and Pt exhibit interactions with the substrate. A detailed discussion for each sample is given in the following sections.

3.2. Au Sample. The XPS spectra of the Au sample exhibit peak positions and intensities for Bi 4*f* and I 3*d* very close to those of the BiI_3 sample. In addition, the Au 4*f* spectrum exhibits the same peak positions as that of pure, metallic gold. These results suggest that Bi, I, and Au maintain their respective chemical states upon formation of the contact interface. In the absence of evidence of chemical reactivity between Au and the BiI_3 (001) surface, Au is taken to be a viable candidate electrode material for use with BiI_3.

Table 1. Observed XPS Binding Energies of the Elements Bi, I, Au, Pd, and Pt

	binding energy (eV)							
peak	BiI_3 sample	Au sample	Pd sample			Pt sample		
Bi $4f_{7/2}$	159.2	159.1	159.2	158.5	157.1	158.9	158.3	157.1
I $3d_{5/2}$	619.4	619.1		619.3		619.4		618.6
Au $4f_{7/2}$		84.0						
Pd $3d_{5/2}$			337.2	336.5	335.0			
Pt $4f_{7/2}$							71.1	

3.3. Pd Sample. Peak shifting within both the Bi 4*f* and Pd 3*d* spectra is observed, which indicates the existence of interfacial reactivity. The iodine peak positions appear at energies very close to those observed from the BiI_3 sample. The deconvolution of Bi 4*f* and Pd 3*d* spectra is shown in Figure 4. In the Bi $4f_{7/2}$ region, three peaks are identified at 157.1, 158.5, and 159.2 eV, consistent with the literature values assigned to bismuth atoms in metallic bismuth,[17] Bi_2O_3,[18] and BiI_3,[15] respectively. However, the assignment of Bi_2O_3 is not stoichiometrically plausible given the amount of oxygen observed in the O 1*s* spectrum. In the O 1s spectrum, the predominant peak intensity actually arises from the Pd $3p_{3/2}$ core level at 533.1 eV.[15] Therefore the most reasonable assignment for the peak at 158.5 eV would be bismuth atoms in a reduced iodine environment (BiI_{3-x} with $x < 3$). The Pd $3d_{5/2}$ spectrum can be deconvoluted into three peaks centered at 335.0, 336.5, and 337.2 eV. These are assigned to palladium atoms in metallic palladium,[15] PdI_2,[17] and PdO,[19] respectively.

The observed metallic Bi and PdI_2 species indicate the occurrence of chemical interactions at the Pd−BiI_3 interface. Pd was also reported to show reactivity with HgI_2 by forming an intermediary layer of PdI_2.[20] This reaction was believed to arise from the reaction of Pd with free iodine produced by the decomposition of HgI_2 over long periods of times.[20,21] However, Pd is still the most commonly used contact material for HgI_2 because of this reactivity issue was believed to only affect the long-term stability of HgI_2 detectors.[4,20] On the basis of the XPS spectra of the BiI_3 sample after exposure to air for one month (Figure 1), it is concluded that BiI_3 does not appreciably decompose to form free iodine, in contrast to HgI_2. Given that the XPS spectra of the Pd sample were measured within one or

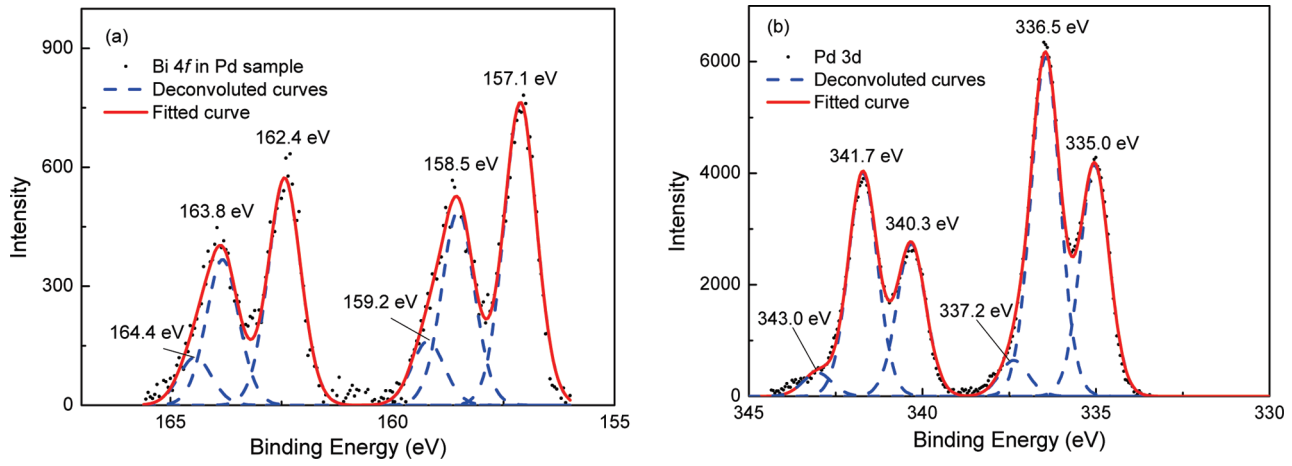

Figure 4. Deconvolution of XPS spectra of Pd sample for (a) Bi 4*f*, (b) Pd 3*d*.

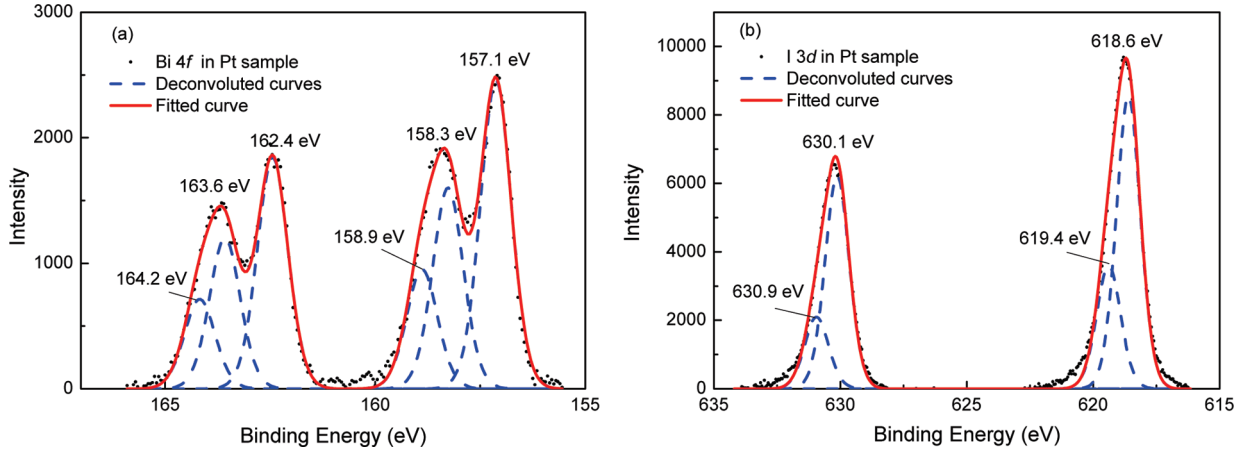

Figure 5. Deconvolution of XPS spectra of Pt sample for (a) Bi 4*f* and (b) I 3*d*.

two days following contact deposition, the formation of PdI_2 suggests direct reactivity with BiI_3.

3.4. Pt Sample. Similar to the Pd sample, peak shifting is observed for the Bi 4*f* peaks measured from the Pt sample. The deconvolution of the Bi 4*f* and I 3*d* spectra from the Pt sample is shown in Figure 5. The assignment of the Bi 4*f* spectrum is made in accord with that of the Pd sample. The Bi $4f_{7/2}$ peaks at 157.1, 158.3, and 158.9 eV were assigned to bismuth atoms in metallic bismuth, BiI_{3-x}, and BiI_3 respectively. The Pt 4*f* spectrum features an asymmetric peak shape, which is indicative of the presence of multiple chemical states for the Pt atoms found in the interfacial region. However, this asymmetry is not believed to be due to reactivity since a similar peak feature is observed in the pure, metallic Pt.[15] Therefore no attempt is made to deconvolute the Pt peaks. The I $3d_{5/2}$ peak is deconvoluted into two peaks at 618.6 and 619.4 eV, given the observed appreciable peak broadening. The peak at 619.4 eV is assigned to iodine atoms in BiI_3, maintaining consistency with the assignments made for the other samples. The peak at 618.6 eV is possibly due to the formation of I_2, implying the decomposition of BiI_3 when in contact with Pt metal.

Similar to Pd sample, chemical reaction is also identified in the sample with Pt electrode. However, the effect of Pt on the surface of BiI_3 is different from that of Pd. Unlike Pd, Pt does not appear to directly form compounds with the other elements involved in the interface. Instead, BiI_3 is observed to decompose in the presence of Pt metal, perhaps in a fashion similar to the decomposition of HgI_2 in the presence of Pd.

3.5. XPS Spectra at Different Take-Off Angles. To provide greater insight into the differing degrees of interfacial reactivity, the photoelectron core-level spectra in the Pd and Pt samples were investigated as a function of takeoff angle. The resulting Bi 4*f*, Pd 3*d*, and I 3*d* spectra and the integrated peak intensities are shown in Figure 6 and Table 2. At higher takeoff angle, the relative intensities of three peaks decreased, the metallic Bi to BiI_{3-x} for the Bi peak, the ratio of metallic Pd to PdI_2, and I_2 to BiI_3. A decrease in relative peak intensity with the increasing takeoff angle is typically observed for subsurface species as a result of the decreased sampling depth for this geometry.[22,23] As discussed above, the appearance of metallic Bi, PdI_2 and I_2 is attributed to an interfacial reaction. The angle dependent results provide additional evidence of this interfacial reactivity and indicate that the reaction products are primarily located at the surface.

3.6. AFM Analysis. AFM characterization was performed on the samples previously studied by XPS to investigate the surface morphology of the metal contacts. Multiple areas were investigated for each sample and the images shown in Figure 7 are

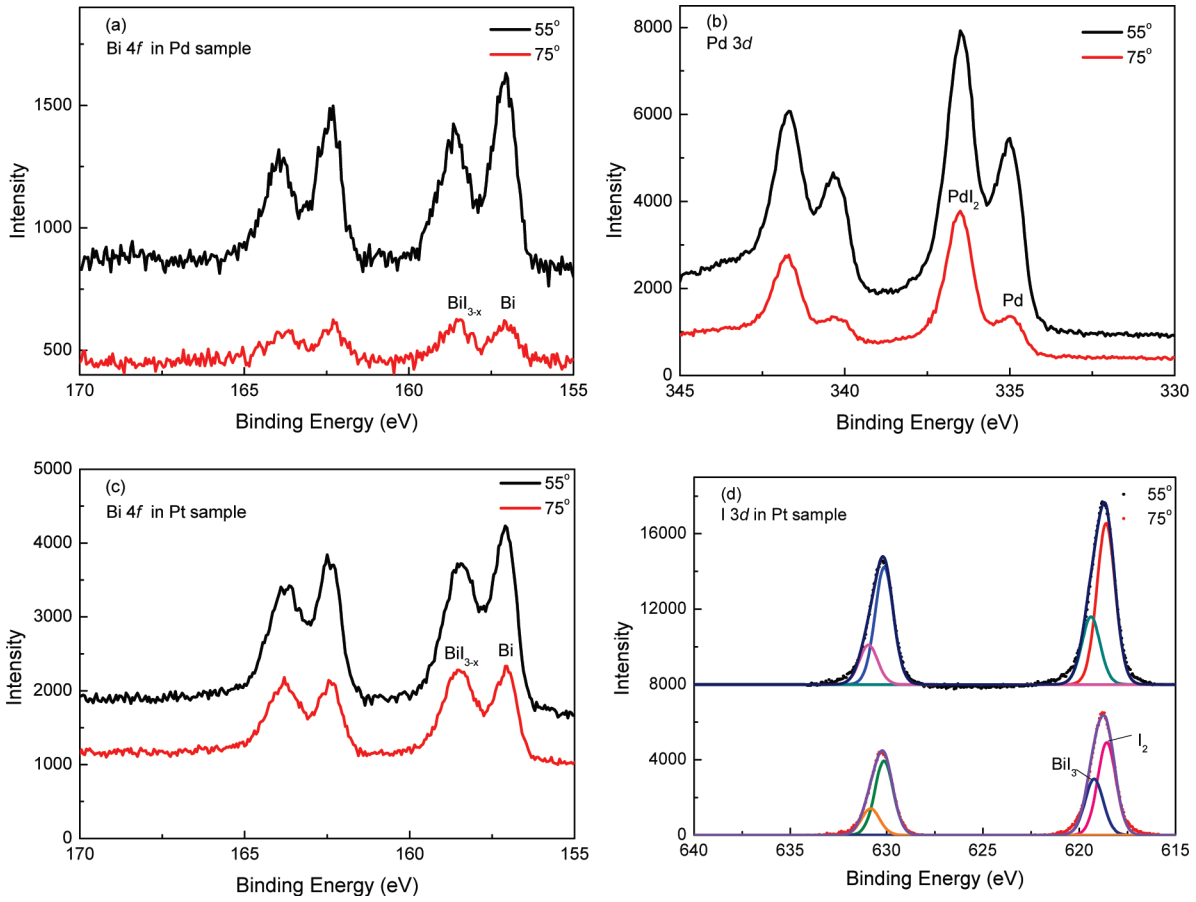

Figure 6. XPS spectra at different takeoff angles: (a) Bi 4*f* in Pd sample, (b) Pd 3*d* in Pd sample, (c) Bi 4*f* in Pt sample, and (d) I 3*d* in Pt sample.

Table 2. Peak Intensities of Core-Level Photoelectrons in Pd and Pt Samples

peak	contact	take-off angle	integrated peak intensity (arb. units)	relative intensity
Bi $4f_{7/2}$ from Bi	Pd	55°	715.9	$Bi/BiI_{3-x} = 1.56$
Bi $4f_{7/2}$ from BiI_{3-x}	Pd	55°	459.9	
Bi $4f_{7/2}$ from Bi	Pd	75°	161.0	$Bi/BiI_{3-x} = 1.04$
Bi $4f_{7/2}$ from BiI_{3-x}	Pd	75°	154.4	
Pd $3d_{5/2}$ from Pd	Pd	55°	4512.0	$Pd/PdI_2 = 0.66$
Pd $3d_{5/2}$ from PdI_2	Pd	55°	6796.7	
Pd $3d_{5/2}$ from Pd	Pd	75°	943.8	$Pd/PdI_2 = 0.29$
Pd $3d_{5/2}$ from PdI_2	Pd	75°	3311.0	
Bi $4f_{7/2}$ from Bi	Pt	55°	2302.7	$Bi/BiI_{3-x} = 1.53$
Bi $4f_{7/2}$ from BiI_{3-x}	Pt	55°	1501.1	
Bi $4f_{7/2}$ from Bi	Pt	75°	1252.8	$Bi/BiI_{3-x} = 1.05$
Bi $4f_{7/2}$ from BiI_{3-x}	Pt	75°	1196.4	
I $3d_{5/2}$ from I_2	Pt	55°	10385.4	$I_2/BiI_3 = 2.38$
I $3d_{5/2}$ from BiI_3	Pt	55°	4364.7	
I $3d_{5/2}$ from I_2	Pt	75°	5975.0	$I_2/BiI_3 = 1.65$
I $3d_{5/2}$ from BiI_3	Pt	75°	3618.0	

representative surface morphologies of the samples. Cursor plots are presented to the right of the AFM images to illustrate representative feature sizes. A stepped surface is observed for the case of the cleaved (001) BiI_3 crystal (Figure 7a). The height of the steps is approximately 0.5 nm, which corresponds to the distance between the I—Bi—I layers within the BiI_3 unit cell. This suggests that the stepped feature is formed by cleaving along different I—Bi—I layers. Upon Au deposition, a complete wetting of the BiI_3 surface is observed in Figure 7b. Although an increased surface roughness (~15 nm) is detected upon deposition, chemically resolved friction force images revealed little contrast and thus no evidence of islanding. For the surface with Pd or Pt electrode, islands with height up to hundreds of nanometers are observed, as illustrated by the bright regions in Figure 7c and d. Pd and Pt both exhibit a nonwetting behavior on BiI_3, likely related to the different reactivities of these metallic species with BiI_3 previously described. As seen in the cursor plots included in Figure 7, the observed surface roughness is much higher for the Au, Pd, and Pt deposits than that observed for the bare BiI_3 sample.

The makeup of the islands can be evaluated by comparing the volumes of the islands and the experimentally deposited thickness metal amount. The volume of the islands is calculated using image processing software (Scanning Probe Image Processing, SPIP^{TM}) to evaluate the histogram of surface heights. The calculated island volume for the Pd sample is 4.6×10^6 nm^3 over a 4 μm^2 area, corresponding to an equivalent thickness of 1.15 nm of evenly distributed Pd. This volume closely corresponds to the experimentally deposited thickness of 1 nm, indicating that the islands are mainly formed of Pd. The island volume of the Pt sample is calculated to be 7.7×10^8 nm^3 over a

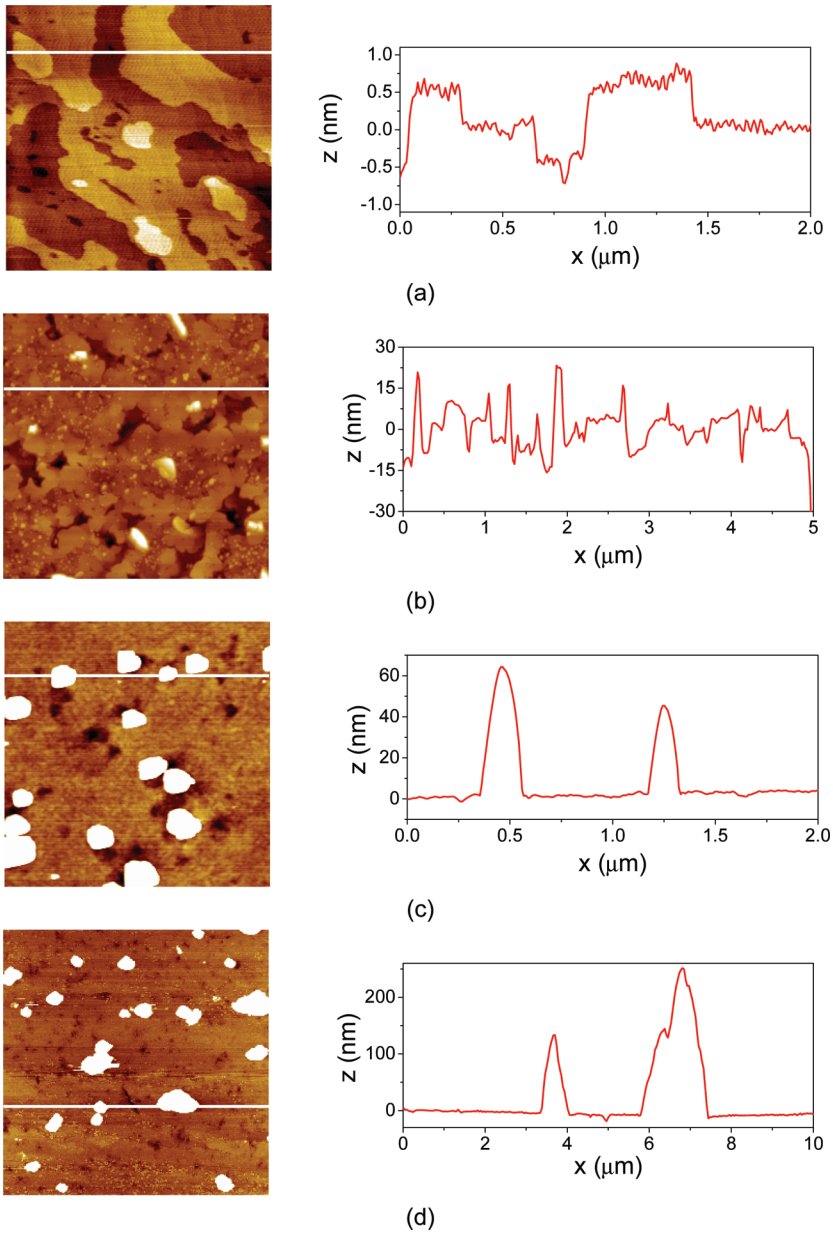

Figure 7. AFM images of topography and cursor plots of (a) BiI_3 single crystal (001) surface, (b) Au sample, (c) Pd sample, and (d) Pt sample. The relative image sizes are indicated by the length of the cursor plots shown to the right of each image. White line in the topographies indicates the position where cursor plot is performed.

100 μm^2 area. This volume would be equivalent to a deposited, evenly distributed thickness of 7.7 nm. This large deviation from the experimental value of 1 nm indicates that interfacial species resulting from the reaction of Pt with BiI3, that is, I_2, heavily contributes to the observed surface morphology, or that the surface has been heavily etched in the process of Pt deposition.

3.7. Physical Models of the Deposited Electrode. As indicated by AFM characterization, both Pd and Pt form islands on the surface of BiI_3. Since the XPS data from section 3.1 provides evidence that Pd forms compound with BiI_3 while Pt does not, different physical models are proposed for the existence of island structures on the Pd and Pt samples.

The model of Pd island formation is illustrated in Figure 8a. At the interface, the strong chemical reaction between Pd and BiI_3 leads to the interdiffusion or reaction of Pd and I to form PdI_2. A layer of metallic Bi is left beneath the forming island. The chemical reaction also takes place at the surface of the Pd islands via surface diffusion of the iodine atoms, leaving partially reduced BiI_{3-x} in regions not covered by islands. The net result is metallic Pd islands encapsulated by PdI_2 distributed across a partially reduced surface. As indicated by the quantitative decrease in metallic Bi intensity at higher takeoff angles discussed in section 3.5, this species primarily resides in regions immediately beneath islands. This is consistent with the majority of surface reduction occurring in the region of island formation. A similar decrease in metallic Pd intensity relative to PdI_2 intensity at higher takeoff angles supports the picture of an encapsulated island with PdI_2 predominantly at the surface.

For the Pt sample, BiI_3 is observed to decompose in the presence of Pt metal. The decomposed metallic Bi and I_2 are

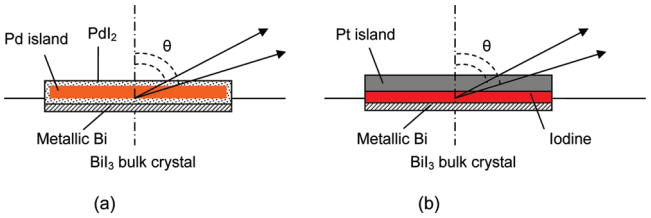

Figure 8. Physical models for electrode islands on the surface of BiI_3 single crystal for the (a) Pd sample and (b) Pt sample. θ is the takeoff angle.

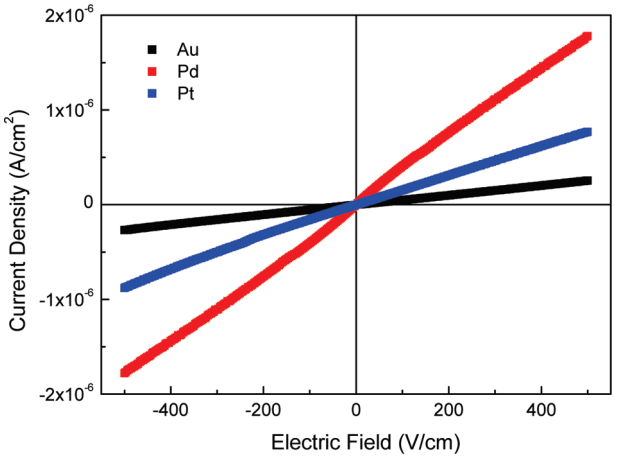

Figure 9. I−V curves for BiI_3 single crystal with Au, Pd, and Pt electrode.

Table 3. Sample Information and Resistivity of BiI_3 Single Crystals for I−V Characterization

electrode	electrode area (cm^2)	thickness (cm)	resistivity 10^9 (Ω·cm)
Au	0.260	0.075	1.85
Pd	0.167	0.075	0.28
Pt	0.251	0.076	0.61

mainly confined underneath the Pt island, consistent with the relatively greater attenuation of the I $3d_{5/2}$ arising from the I_2 species as compared to that from BiI_3 found in regions apart from island formation.The hierarchy of this model is proposed as a sandwich structure of Pt−I_2−Bi layer stacked from top to bottom, as illustrated in Figure 8b. The formation of an I_2 layer increases the total height of the island and accounts for the higher equivalent thickness of the islands estimated by the AFM. On the basis of this model, the relative intensity of the metallic Bi and I_2 will decrease at higher takeoff angle as subsurface species, in agreement with the observed XPS results.

3.8. I−V Characterization. The resistivity of BiI_3 single crystals has been measured following deposition of Au, Pd, and Pt electrodes. The crystal samples were cut from adjacent positions in a larger single crystal BiI_3 to minimize the sample variation. The I−V curves for crystals with different electrodes are shown in Figure 9. It is observed that the crystal with Au electrodes has the highest resistivity, (1.85×10^9 Ω·cm) and the one with Pd electrodes shows the lowest, (0.28×10^9 Ω·cm). These results are summarized in Table 3. Fornaro et al. also reported that BiI_3 crystal showed higher resistivity with Au electrodes than with Pd electrodes, where the crystals were grown by PVT method and the electrodes were deposited by evaporation.[2] This suggests that the resistivity variation is independent of the crystal growth and electrode deposition technique, and is most likely caused by the interactions between the electrode material and the semiconductor. Given that the metallic Bi is identified at the Pd−BiI_3 interface, it is possible that Bi atoms diffuse into the subsurface region of the crystal and affect the metal-semiconductor barrier. On the basis of the XPS results, Au is expected to be physically in contact with BiI_3. Thus, the measured resistivity represents a more accurate value for this material. The sample with a Pt electrode shows a measured resistivity value between Au and Pd (0.61×10^9 Ω·cm). In general, it is concluded that the resistivity of the coated BiI_3 single crystals scales inversely with the degree of interfacial reactivity.

4. CONCLUSIONS

XPS characterization indicates that sputtered Pd and Pt have chemical interactions with the BiI_3 (001) surface, while Au is observed to be unreactive with BiI_3. Upon deposition, Pd is observed to react with BiI_3 to form metallic Bi and PdI_2. Pt does not react with BiI_3 to form a distinguishable compound but appears to induce the decomposition of BiI_3. Based upon angle resolved XPS data and the volumetric analysis of the AFM topographic data, two different detailed physical models are proposed for the Pd and Pt island formation. The I−V characterization corroborates the XPS result, and the highest resistivity is obtained from a sample with Au electrodes. It is concluded that Au is a better candidate electrode material for BiI_3 single crystal over Pd and Pt.

■ ACKNOWLEDGMENT

This research is supported in part by DOD, Defense Threat Reduction Agency (Contract HDTRA 10710013) and DOE/NNSA Grant no. DE-FG52-09NA29358.

■ REFERENCES

(1) Matsumoto, M.; Hitomi, K.; Shoji, T.; Hiratate, Y. *IEEE Trans. Nucl. Sci.* **2002**, *49* (5), 2517–2520.
(2) Fornaro, L.; Cuna, A.; Noguera, A.; Perez, M.; Mussio, L. *IEEE Trans. Nucl. Sci.* **2004**, *51* (5), 2461–2465.
(3) Schlesinger, T. E.; Toney, J. E.; Yoon, H.; Lee, E. Y.; Brunett, B. A.; Franks, L.; James, R. B. *Mater. Sci. Eng., R* **2001**, *32* (4−5), 103–189.
(4) Piechotka, M. *Mater. Sci. Eng., R* **1997**, *18* (1−2), 1–98.
(5) Dmitriev, Y. N.; Bennett, P. R.; Cirignano, L. J.; Klugerman, M.; Shah, K. S., presented at the SPIE Conference on Hard X-Ray, Gamma-Ray, and Neutron Detector Physics, 1999, *3768*, 521−529.
(6) Fornaro, L.; Saucedo, E.; Mussio, L.; Gancharov, A.; Cuna, A. *IEEE Trans. Nucl. Sci.* **2004**, *51* (1), 96–100.
(7) Gerrish, V. M. In *Semiconductors for Room Temperature Nuclear Detector Applications*; Schlesinger, T. E., James, R. B., Eds.; Academic Press: San Diego, CA, 1995; Vol. 43, p 520.
(8) Bao, X. J.; Schlesinger, T. E.; James, R. B.; Stulen, R. H.; Ortale, C.; van den Berg, L. *J. Appl. Phys.* **1990**, *67* (12), 7265–7267.
(9) James, R. B.; Bao, X. J.; Schlesinger, T. E.; Cheng, A. Y.; Gerrish, V. M. Presented at the Materials Research Society, San Francisco, 1993, *302*, 103.
(10) Cheng, A. Y. Presented at the Material Research Society, San Francisco, 1993, *302*, 141.
(11) Dharmadasa, I. M. *Prog. Cryst. Growth Charact. Mater.* **1998**, *36* (4), 249–290.

(12) Marinelli, C.; Sorba, L.; Muller, B. H.; Kumar, D.; Orani, D.; Rubini, S.; Franciosi, A.; De Franceschi, S.; Lazzarino, M.; Beltram, F. *J. Cryst. Growth* **1999**, *202*, 769–772.
(13) Velasquez, P.; Leinen, D.; Pascual, J.; Ramos-Barrado, J. R.; Cordova, R.; Gomez, H.; Schrebler, R. *J. Electroanal. Chem.* **2001**, *510* (1−2), 20–28.
(14) Moroseac, M.; Skala, T.; Veltruska, K.; Matolin, V.; Matolinova, I. *Surf. Sci.* **2004**, *566*, 1118–1123.
(15) Moulder, J. F.; Stickle, W. F.; Sobol, P. E.; Bomben, K. D. In *Handbook of X-ray Photoelectron Spectroscopy*, 2nd ed.; Chastain, J., King, R. C., Eds.; ULVAC-PHI, Inc.: Chanhassen, 1995, p 215.
(16) Shirley, D. A. *Phys. Rev. B* **1972**, *5* (12), 4709–4714.
(17) Ismail, F. M.; Hanafi, Z. M. *Z Phys Chem-Leipzig* **1986**, *267* (4), 667–672.
(18) Schuhl, Y.; Baussart, H.; Delobel, R.; Lebras, M.; Leroy, J. M.; Gengembre, L.; Grimblot, J. *J. Chem. Soc., Faraday Trans. 1* **1983**, *79*, 2055–2069.
(19) Fleisch, T. H.; Mains, G. J. *J. Phys. Chem.* **1986**, *90* (21), 5317–5320.
(20) Schieber, M.; Schlesinger, T. E.; James, R. B. In *Semiconductors for Room Temperature Nuclear Detector Applications*; Schlesinger, T. E., James, R. B., Eds.; Academic Press: San Diego, CA, 1995; Vol. 43, p 571.
(21) Scott, R. S.; Fredericks, G. E. *Appl. Phys. Lett.* **1975**, *27* (2), 99–100.
(22) Gunter, P. L. J.; Dejong, A. M.; Niemantsverdriet, J. W.; Rheiter, H. J. H. *Surf. Interface Anal.* **1992**, *19* (1−12), 161–164.
(23) Aarnink, W. A. M.; Gao, J.; Rogalla, H.; Vansilfhout, A. *J. Less-Common. Met.* **1990**, *164*, 321–328.